THE JOURNAL OF PHYSICAL CHEMISTRY B

Article

pubs.acs.org/JPCB

Probing the Thermal Collapse of Poly(*N*-isopropylacrylamide) Grafts by Quantitative *in Situ* Ellipsometry

E. Stefan Kooij,*[,†] Xiaofeng Sui,[‡] Mark A. Hempenius,[‡] Harold J. W. Zandvliet,[†] and G. Julius Vancso*[,‡]

[†]Physics of Interfaces and Nanomaterials, MESA+ Institute for Nanotechnology, University of Twente, P.O. Box 217, 7500AE Enschede, The Netherlands

[‡]Materials Science and Technology of Polymers, MESA+ Institute for Nanotechnology, University of Twente, P.O. Box 217, 7500AE Enschede, The Netherlands

Supporting Information

ABSTRACT: We demonstrate the potential of *in situ* spectroscopic ellipsometry for the investigation of the chain segment density profile and layer thickness during the temperature-induced, reversible collapse−expansion transition of poly(*N*-isopropylacrylamide) (PNIPAM) grafted layers. Here, we study PNIPAM films with variable grafting densities in aqueous systems, which were produced by atom-transfer radical polymerization (ATRP). In our attempt to obtain a realistic quantitative description of the thickness of our swollen PNIPAM layers, various models were implemented to fit the ellipsometric data. As expected, we found that the swelling ratio is strongly dependent on the grafting density. From the ellipsometry results, the density and thickness variation accompanying the collapse transition across the lower critical solution temperature (LCST) was characterized. The collapse can be adequately explained by considering the PNIPAM film to consist of two layers: (i) a dense layer near the surface and (ii) a more diluted layer on the side of the film exposed to the solvent. Analysis of the optical response reveals a gradient density profile within these layers.

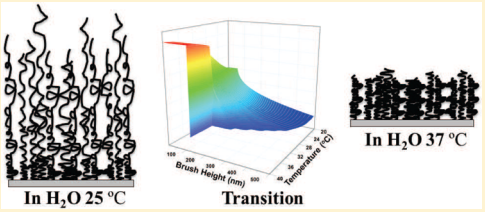

INTRODUCTION

Stimuli responsive polymer layers consisting of surface-tethered macromolecules have been widely applied to prepare sensors, to regulate cell cultures, to control wetting and adhesion, and in many other areas.[1−8] The thermally induced collapse transition of poly(*N*-isopropylacrylamide) (PNIPAM) in aqueous liquids and also in mixed solvents has been investigated extensively. As a responsive polymer, PNIPAM is one of the most frequently studied entities.[9−11] At temperatures below the lower critical solution temperature (LCST), the polymer is soluble in water due to *cooperative hydration*,[12−14] which is caused by a positive correlation between adjacent bound water molecules. Due to steric interactions, consecutive sequences of bound water appear along the PNIPAM molecule. Upon heating the system to temperatures above the LCST, which is around 32 °C in aqueous media, each sequence is considered to collectively dehydrate, resulting in a collapse of the grafted molecules. PNIPAM chains show strong hydration behavior below the LCST, while above the LCST they adopt a dehydrated and compact form (as schematically shown in Scheme 1). By utilizing the hydration/dehydration effect, PNIPAM layers are expected to have applications in, e.g., permeation-controlled filters, tissue engineering, and actuators.[15−19]

Over the past decades, different models describing the equilibrium conformation of polymers attached by one end to a substrate and immersed in a solvent have been described. Generally, the grafted polymers are considered to consist of segments, the behavior of which is determined by the balance of various interactions (segment−segment and segment−solvent) in the solvent. In the pioneering work by Alexander and De Gennes,[20−22] the polymer grafts are modeled by a step-like concentration profile, in which the segment density is considered constant throughout the layer. Within the Alexander−De Gennes constant density model, all free chain ends are estimated to be at the same distance from the surface, therewith imposing severe restrictions on the allowed polymer chain configurations. To circumvent these restrictions, more recently self-consistent field approximations have been used to numerically derive concentration profiles within the polymer thin films.[23,24] Depending on the specific interactions between the polymer and the solvent, various different gradient profiles have been reported.[23−25]

Thermoresponsive Surface Immobilized PNIPAM Films. The influence of temperature on the polymer structure and hydration of PNIPAM films in water is well-documented in the literature. Several methods, including atomic force microscopy (AFM),[26−35] surface force measurements,[36,37] neutron reflectivity,[38,39] quartz-crystal microbalance,[28,40−42] optical micromanipulation technique,[43] ellipsometry,[35,44−48] and surface plasmon resonance,[49,50] have been used to monitor the reversible thermoresponsive properties for PNIPAM films in solution with different densities and molar masses.

Different ways to immobilize PNIPAM entities at well-defined interfaces have been described. One class of polymeric

Received: May 5, 2012
Revised: June 19, 2012
Published: July 17, 2012

   dx.doi.org/10.1021/jp304364m | J. Phys. Chem. B 2012, 116, 9261−9268

Scheme 1. (top left) Schematic Representation of PNIPAM Chains Grafted from an Oxide Surface; (top right) Typical AFM Topographic Image and Profile of a Dry MD PNIPAM Film as Used in This Work; (bottom) Schematic Representation of Differences in Conformation of PNIPAM Thin Films at Temperatures below (left) and above (right) the LCST

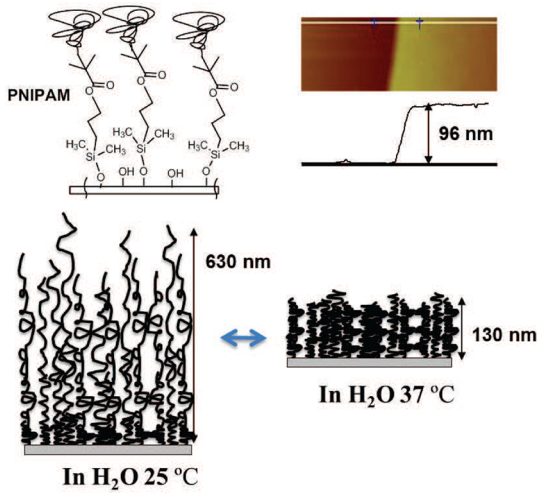

materials comprises hydrogels, either in the form of a homogeneous layer, microstructured arrays, or sub-micrometer-sized particles.[26,46,48,50−53] Owing to varying degrees of cross-linking within the films, the LCST in these materials is markedly different from those typically observed in PNIPAM brushes. Polymer brushes in general, and also more specifically PNIPAM grafts, can be prepared by two main approaches, generally referred to as "grafting to" and "grafting from".[8] In the former technique, well-defined, preformed polymer chains, which can be designed and functionalized for specific potential applications, are attached to a surface. Due to steric hindrance, only low grafting densities and therewith films with thicknesses in the low nanometer range have been reported.[31,37,39,44] As such, the contribution from collective behavior arising from interchain interactions to the swelling and deswelling behavior of these low-density brushes will be relatively small.[44] Moreover, in contrast to brush films with a high grafting density, the lower densities in "grafted to" brushes allow for intermediate regimes during the collapse transition, such as the "mushroom" conformation. Overall, the relatively small amount of polymer chains tethered to the substrate surface poses an experimental challenge in the elucidation of a detailed mechanism for the collapse transition of such surface immobilized PNIPAM brushes.

In the "grafting from" approach, surface-tethered initiating sites are used from which polymeric chains are grown. This method allows control over the surface concentration of active sites and potentially yields markedly higher grafting densities. Recent advances in the controlled free radical polymerization have enabled the use of a wide variety of monomers, including PNIPAM. In some of the reports in the literature using "grafted from" PNIPAM brushes, the focus is only on the limiting states well below and well above the bulk transition temperature.[29,32]

In a number of papers focused on *in situ* studies of the actual transition,[16,28,30,34−36,38,40−45,47−49,54,55] it has been shown in detail that the properties of PNIPAM layers can be strongly affected by grafting density, molecular weight, polydispersity, and solvent composition. For PNIPAM brushes, a broad rather than a sharp coil−globule transition was described. The origin of this gradual transition process is ascribed to the nonuniformity of the PNIPAM brushes as well as the cooperativity of intra- and intermolecular hydrogen bonds between collapse and dehydration transitions. These observations are consistent with theoretical predictions by Zhulina et al.,[56] who show that, due to repulsive interactions between densely grafted stretched chains, the collapse of a dense planar brush is accompanied by a continuous solubility transition.

Ellipsometric Characterization of the Collapse Transition. In this work, we use ellipsometry in an attempt to quantitatively characterize the variation of the thickness of and the density profile across "grafted from" PNIPAM layers with temperature during the thermally induced collapse. As such, our experiments complement frequently used but considerably more complex neutron reflectivity measurements.[54,55,57] Ellipsometry comprises a powerful, noninvasive optical probe enabling characterization of bulk materials as well as thin films in terms of a number of (structural) material properties. As such, it has been widely used for studies of polymer layers under different conditions.[47,58−60] However, in the vast majority of studies, single wavelength ellipsometry is used,[45,46] rendering it difficult to unambiguously analyze the data in terms of a detailed model incorporating (optical) density profiles. As an example, Edmondson et al.[58] performed *in situ* ellipsometric measurements to study the cononsolvency effect, i.e., the collapse in a mixed water−methanol solvent, of poly(2-(methacryloyloxy) ethyl phosphorylcholine) (PMPC) brushes. Their results show that the judicious selection of the model is essential for extracting meaningful information. It was found that the best fits to the experimental data were obtained using an exponential decay of polymer density away from the surface.

Spectroscopic ellipsometry has been used in several investigations on PNIPAM films in different surface states, i.e., hydrogels or brushes. Spectroscopic ellipsometry involves the measurement of the optical response in terms of ellipsometric parameters over a wide spectral range. A number of studies have focused on PNIPAM-containing hydrogels.[51−53] Schmaljohann et al. report the use of imaging ellipsometry on micropatterned hydrogels.[48] In all these cases, the optical response of the PNIPAM-containing hydrogel layers was modeled using a single homogeneous film, often by using a Cauchy model to account for the wavelength dispersion in combination with an effective medium approximation to accommodate contributions from defects or vacancies within the film. In one report, it is specifically stated that a gradient layer model is not possible owing to the large number of fit parameters.[52]

More specifically pertaining to PNIPAM brushes, spectroscopic ellipsometry has been used both on PNIPAM brushes "grafted from"[15,35,61] and also "grafted to"[44] suitable substrates. In reports on the former method, a single homogeneous Cauchy layer is used, while in the latter case a multilayer box model is used, also in combination with the Cauchy model. To account for the swelling behavior, the Bruggeman effective medium approximation was used to describe the different polymer volume fractions.

Surprisingly, in none of these papers actual ellipsometry spectra are presented, and also the quantitative discussion of the fit results does not reflect fine details of the brush density in the normal direction of the films. Here, we use *in situ*

ellipsometry in spectroscopic mode to study the thermally induced collapse of PNIPAM entities, grafted from the substrate with different grafting densities as a function of phase state across the LCST in real time. The ellipsometry results are analyzed in terms of a model involving a bilayer gradient density profile, which adequately fits the data, therewith enabling a quantitative discussion of the reversible thickness of our brushes with varying temperature.

EXPERIMENTAL DETAILS

Materials. PNIPAM films with three different grafting densities, referred to as high, middle, and low density (hereafter designated as HD, MD, and LD, respectively) are synthesized via surface-initiated atom-transfer radical polymerization (SI-ATRP).[62] The grafting densities amount to approximately 0.69, 0.27, and 0.03 chains/nm^2 for the three types of samples considered in this work. These values were estimated using a previously reported procedure,[28,63] by measuring the dry thickness and molar mass of the free polymer (M_n = 219600 g/mol; M_w = 519300 g/mol) obtained using "sacrificial" initiators in the polymerization mixture.[15] A direct measurement of the grafting density and the polymer chain length is difficult due to the very small amount of polymer chains at the surface. The aforementioned method only provides a rough estimate of the molecular weight and therewith also for the grafting densities. The water used in all experiments was of Milli-Q grade (Millipore; 18.2 MΩ cm).

Measurements. The optical experiments were performed using a Woollam variable angle spectroscopic ellipsometer (VASE) system. Measurements were carried out as a function of photon energy in the range 1.5−4.5 eV with a step size of 0.1 eV; this corresponds to a wavelength range of 275−827 nm. All experiments were done *in situ* using a custom-built, dedicated temperature-controlled cell. Optical access to the sample was achieved through two windows at a fixed angle of incidence θ = 63°. A third window enabled alignment of the sample at normal incidence as well as allowed visual inspection of the sample during *in situ* experiments. Temperature control was achieved using an externally heated bath from which water was continuously pumped to the cell; the temperature was stabilized using a thermostat sensor inside the liquid cell, not more than 1 cm from the sample under investigation. In all cases, the temperature was stable within ±0.5° during measurement of the spectra, typically a few minutes.

In reflection ellipsometry, the change in the polarization state of light with a well-defined polarization upon reflection at an interface is measured. The complex reflection coefficient ρ is defined as

$$\rho = \frac{r_p}{r_s} = \tan\Psi \exp(i\Delta) \quad (1)$$

where r_p and r_s are the complex reflection coefficients for the parallel and perpendicular polarizations, respectively.[64] The amplitude ratio is expressed by tan Ψ, while Δ represents the phase difference. The ellipsometry spectra, i.e., Ψ and Δ as a function of wavelength, were analyzed using the package CompleteEASE (Woollam), employing tabulated dielectric functions for silicon, silicon dioxide, and water.[65] In all cases, the Levenberg−Marquardt multivariate regression algorithm was applied in the fitting procedure.

Ellipsometric Characterization of the Grafted Polymer Thin Films. Typical ellipsometry spectra at different temperatures are shown in Figure 1 for a MD sample; comparable spectra for LD and HD are available in the Supporting Information. Three spectra are shown corresponding to temperatures (i) well below, (ii) near, and (iii) well above the LCST. The variation of the spectra with temperature is obvious from Figure 1, showing the optical signature of the temperature-induced LCST transition. For the swollen state at relatively low temperatures (squares), features of the silicon substrate can be identified in the spectra, such as the peak in Ψ near 3.4 eV and the decreases of Δ near 3.3 and 4.3 eV. Owing to the large swelling in water, which is accompanied by a considerably reduced (optical) density of the polymer as compared to that of its collapsed wet or dry conformation, the contribution of the swollen polymer film to the optical spectra becomes hard to distinguish from the solvent, i.e., water. The refractive index of the swollen, diluted polymer is described by an effective medium approximation incorporating the refractive indices of water and the PNIPAM molecules. Assuming a low PNIPAM concentration in the relatively thick diluted layer, its effective refractive index is only slightly larger than that of water, and approximately a linear function of the polymer concentration.

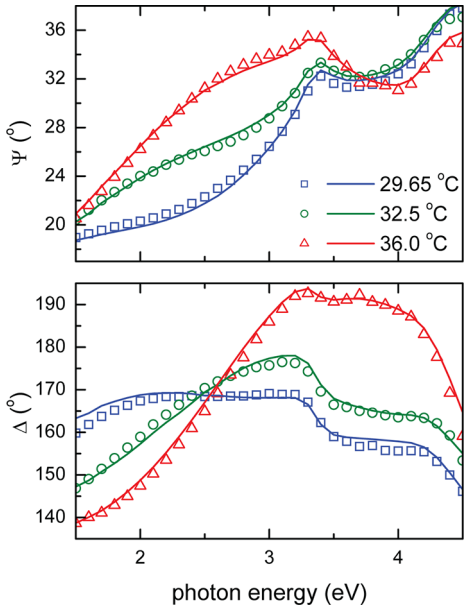

Figure 1. *In situ* ellipsometry spectra on a MD PNIPAM grafted layer at temperatures well below (blue; squares), near (green; circles), and well above (red; triangles) the LCST. The data points represent experimental results, while the solid lines are simulated spectra as described in the text.

Heating of the system across the LCST gives rise to marked changes in the spectra. A shoulder develops at Ψ values below 3.0 eV, while Δ decreases with temperature below 2.5 eV and increases markedly at higher photon energies. From these results, it is obvious that measurements at a single wavelength, as is common with *in situ* ellipsometry, make it impossible to unambiguously analyze the data. The fact that the temperature response of the system in terms of optical properties depends strongly on photon energy (and thus also wavelength) is clearly shown in Figure 2.

Typically, it takes a few minutes to measure spectra such as those shown in Figure 1, owing to the relatively slow scan rate of the monochromator and the required integration time at all

dx.doi.org/10.1021/jp304364m | J. Phys. Chem. B 2012, 116, 9261−9268

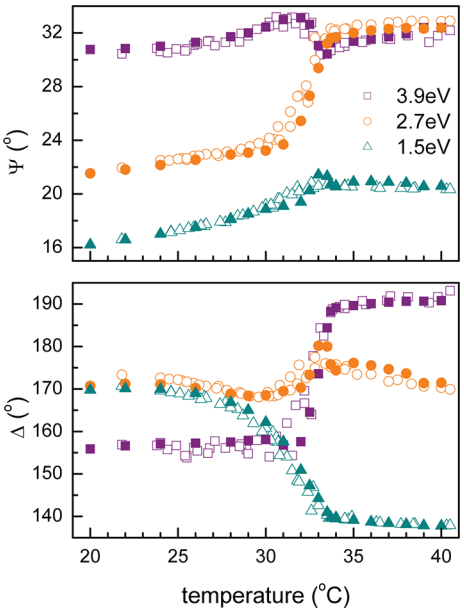

Figure 2. Temperature dependence of the ellipsometric quantities Ψ and Δ (top and bottom panels, respectively) at three different photon energies for the MD brush: 3.9 eV (320 nm; purple squares), 2.7 eV (460 nm; orange circles), and 1.5 eV (825 nm; cyan triangles). The open and filled symbols represent experimental and simulated data, respectively.

energy values. To characterize the relatively fast transition of PNIPAM, this may be too slow. As such, we have also performed measurements at specific photon energies, keeping the monochromator at a fixed position, while continuously monitoring the temperature in our cell during heating/cooling cycles. In this way, the time resolution of the experiments is substantially improved.

The experimental results in Figure 2 for the MD sample (results for the HD and LD samples are provided in the Supporting Information) reveal that at temperatures (i) below approximately 25 °C and (ii) above 35 °C the optical response of the PNIPAM thin films is different but essentially independent of temperature. The most pronounced changes in the optical response occur near 32−33 °C, in good agreement with many of the reports on PNIPAM available in the literature.[35,42,43,47−49] However, in the temperature range 25−30 °C, already a significant change in the optical properties can be discerned. We will provide a possible explanation for this behavior in the next section, in which we present the analysis of the spectra in terms of a quantitative model.

On the basis of the results such as those shown in Figure 2 (see also the Supporting Information), it is not possible to identify a single transition temperature, contrary to bulk PNIPAM. However, the endset of the collapse transition, i.e., during heating, occurs at temperatures of 33.9, 32.9, and 32.8 °C for the HD, MD, and LD samples, respectively. These values are within the typical range often reported in the literature, and slightly higher than the generally established bulk LCST value of 32 °C.[10]

Also shown in Figure 2 are results from the simulated spectra based on the analysis as presented in the next section at fixed temperatures. The pronounced similarity between the measured and simulated data (open and filled symbols, respectively) demonstrates that at all temperatures the system is in equilibrium.

Analysis of the Spectra. We start the analysis of the ellipsometry spectra by considering the two limiting cases, i.e., at temperatures well below and well above the collapse transition. For the high temperature situation, the optical response of the collapsed films can be modeled using a single layer. The refractive index of this layer is adequately described using a Cauchy model[64] for the refractive index n:

$$n(\lambda) = A + B/\lambda^2 + C/\lambda^4 \quad (2)$$

where we consider the wavelength λ in micrometers. We neglect absorption, i.e., the imaginary part of the complex refractive index $k = 0$; as such, we consider the films to be fully transparent. The quantities A, B, and C represent fit parameters. In the present work, we set $C = 0$, since varying it does not yield better fit results.

In the modeling of the optical response of the collapsed films, a minor improvement can be obtained by including a gradient of the Cauchy parameter A as a function of distance from the substrate. A decrease of the value of A by 2% across the thickness of the brush film (from a value higher than the average at the film/substrate interface to a lower value at the film/liquid interface) yields a slightly better fit, reflecting a small but discernible segment density gradient within the film. Nevertheless, to simplify the analysis and to keep the number of fit parameters limited, we neglect here this gradient and consider the Cauchy layer to be homogeneous throughout the collapsed PNIPAM film, as schematically shown in the right part of Scheme 2.

Scheme 2. Schematic Representation of the PNIPAM Segment Density Variation at Temperatures below (left) and above (right) the LCST[a]

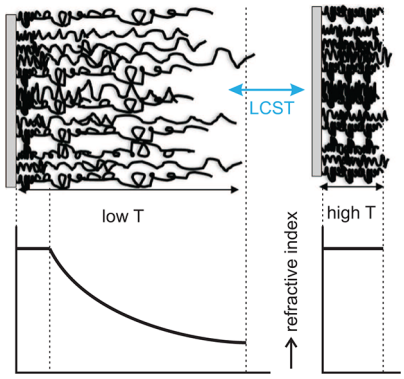

[a]The corresponding refractive index as a function of distance from the substrate is also schematically shown. At low temperatures, the brush film is modeled by a double layer, with the outer exhibiting a gradient density profile; at high temperatures, only a single layer with a constant refractive index is considered, as discussed in the text.

For the swollen PNIPAM films at temperatures below the LCST, adequate fitting is only possible when using a two-layer model, as schematically outlined in the left part of Scheme 2. At the substrate side of the polymer layer, i.e., where the PNIPAM molecules are grafted to the substrate, a layer with a constant segment density is considered in the model, with optical properties similar to those of the collapsed film at higher temperatures. On top of this dense layer, a second layer with a marked gradient in the A-parameter (eq 2), representing the decreasing segment density, is included in the model. We assume a large contribution originates from an intrinsic gradient

dx.doi.org/10.1021/jp304364m | J. Phys. Chem. B 2012, 116, 9261−9268

related to a depth distribution of the chain ends, and to the length distribution of the chains. The gradient in the optical density is described by an exponential decrease of the constant A as used in the Cauchy expression, i.e., $A \propto (d/d_0)^t$, with d the distance within the film, normalized to the total thickness d_0; the exponent t is also a fit parameter. In the left part of Scheme 2, the exponentially decreasing refractive index is schematically shown. Using this model, the ellipsometry spectra can be adequately modeled, as shown by the solid lines in Figure 1 (more spectra and fits are available in the Supporting Information).

An important fit parameter is the thickness of the PNIPAM film, comprising the sum of the thicknesses of the dense layer at the substrate side and the more dilute, gradient layer at the solvent side. Note that the effective thickness follows from the fit model used in the analysis of the ellipsometry spectra. In Figure 3, the temperature dependence of the thickness for both

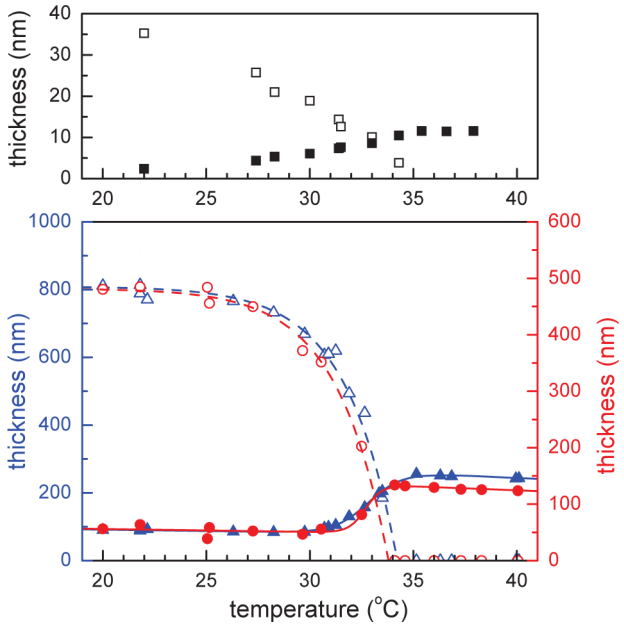

Figure 3. Temperature dependence of the PNIPAM brush thickness as determined from fitting the ellipsometry spectra. In the analysis, the optical response of the PNIPAM films is modeled using a two-layer structure, consisting of a dense, constant segment (optical) density layer (filled symbols) near the substrate and a more diluted layer on the liquid side (open symbols), exhibiting a decrease of polymer segment density with increasing distance from the substrate. Results are shown for LD (top panel), MD, and HD samples (circles/right/red and triangles/left/blue axes of the bottom panel, respectively). The solid and dashed lines represent the temperature dependencies of the thickness of the dense and diluted layers, respectively; analytical expressions for these lines are provided in the Supporting Information.

layers is shown for LD (top panel), MD, and HD brushes (bottom panel). The LD film exhibits a relatively smooth transition with temperature, but we note that the accuracy is rather poor due to the inability to unambiguously model both the thickness and the refractive index. For the LD sample, the experiment for such low thicknesses is only sensitive to the product of thickness and refractive index.

For the MD and HD samples (red circles and blue triangles, respectively), the thickness values exhibit very similar behavior as a function of temperature. Comparing the left and right axes, the thickness values for the MD and HD PNIPAM films appear to scale by a factor of approximately 1.7. At temperatures below 25 °C, the thickness for both films is constant. The latter is in line with the results of Figure 2, which do not exhibit any marked change of the optical response for temperatures below 25 °C.

With increasing temperature, the thickness of the dilute, gradient layer decreases until this layer "vanishes" above 33−34 °C. Zooming in on the thickness of the dense layer (not shown), a very slight decrease of the thickness can be discerned for temperatures up to 30 °C. At first, this may not seem significant. However, close inspection of the results in Figure 2, and more specifically the data for 1.5 and 2.7 eV photon energy, reveal a slight variation of the optical response, most likely related to the thickness variation. Upon further heating, an increase of the thickness of the dense layer is observed simultaneously with the collapse of the dilute layer. At temperatures above 35 °C, only the dense layer remains, the thickness of which again exhibits a minor decline with temperature.

Using the model described above, we have been able to parametrize all fitting parameters, which in turn can be used to calculate the complete optical response as a function of temperature. This enables us to simulate the temperature response of the Ψ and Δ values. For the MD brush, in Figure 2, the simulated values (closed symbols) are compared to the experimental results (open symbols). There is good agreement between the experimental data and the simulated values, confirming the accuracy of our model. At temperatures close to the most pronounced transition, small features in the simulated data can be discerned which are not seen in the experimental data, most likely due to the limited energy resolution of the monochromator of the ellipsometer. Details pertaining to the model, including all equations describing the parametrization, are available in the Supporting Information.

(Optical) Density Profiles. The parametrization of the optical response of our PNIPAM films as a function of temperature in terms of graded optical properties enables us to plot the optical density profile throughout the film thickness for different temperatures. Assuming that these correspond in some way (most likely nonlinear) to the mass density in the film, a variation of the segment density in the film normal direction across the LCST and a refined molecular scale picture of the phase transition within our films can be proposed. In Figure 4, the density profiles for the HD, MD, and LD samples are shown at different temperatures. The profiles demonstrate that, upon increasing the temperature across the LCST, the dense layer increases in thickness (as in Figure 3), while a slight increase of its density is observed. Surprisingly, the refractive index variation for the MD film is markedly larger than that for the HD sample; apparently, the collapse of the polymer segments within the constant density layers is more pronounced for lower grafting densities. For the LD brush, this increase is absent, since we were not able to fit this parameter for these films; we took a constant value for the refractive index of this layer.

The graded, dilute outer layer exhibits a density gradient, with a decay from the value of the dense layer, to a value almost that of the water. As such, although the optical modeling yields a well-defined thickness, the exact position of the dividing interface in the actual experiment is difficult to define. From the profiles in Figure 4, it directly follows that the collapse occurs by a simultaneous decrease of the thickness of the gradient segment layer and a growth of the constant segment density

dx.doi.org/10.1021/jp304364m | J. Phys. Chem. B 2012, 116, 9261−9268

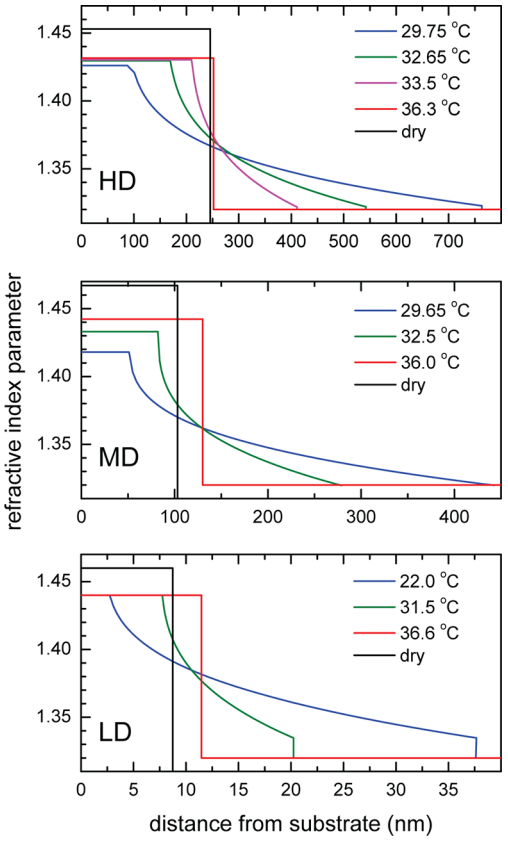

Figure 4. Refractive index profiles as a function of distance from the substrate for our HD (top), MD (middle), and LD (bottom) PNIPAM brush samples; note the different distance scales in the panels. The refractive index is represented by the first Cauchy parameter *A* as described in the text. Results are shown for dry brushes (solid line) and for samples in contact with water at different temperatures. Profiles well below and above the LCST are represented by blue and red lines, respectively; specific temperatures for the different samples are indicated in each panel.

layer at the substrate side of the film, in agreement with the thickness variation as shown in Figure 3.

Similar behavior in terms of a dense layer growing at the expense of a more dilute outer layer has been suggested previously both for PNIPAM films[35,42,49,55] as well as for thermoresponsive PEG-based brushes.[57,66] Pertaining to the latter system, in a recent study,[66] the collapse transition of a temperature responsive brush consisting of poly[di(ethylene glycol) methyl ether methacrylate] ($PMEO_2MA$; grafting density estimated at 0.3 nm^{-2}) was monitored using a combination of quartz crystal microbalance and contact angle measurements. From their experiments, Laloyaux et al.[66] concluded that the *bulk* of the brush collapsed over a broad temperature range and the end of the transition was signaled by a sharp variation of the properties of the *outer surface* of the brush.

More specific to our work described here, Balamurgan et al.[49] characterized "grafted from" PNIPAM brushes and obtained essentially the same results. Unfortunately, the grafting density and molecular weight were not reported, but the films have a relatively large dry thickness of 50 nm indicating grafting densities comparable to our samples. Using the surface plasmon resonance technique, the authors observed a gradual change of the brush thickness with temperature, while the contact angle measurements exhibited an abrupt change around 32 °C. A bilayer profile was proposed by these authors for the graft morphology assuming that the *outermost* region of the brush remains highly solvated at temperatures below the LCST, while the densely packed, less solvated segments in the brush *interior* undergo dehydration over a much broader temperature range.

To the best of our knowledge, three reports in the literature describe the thermoresponsive behavior of PNIPAM films very similar to the ones we consider here. Plunkett et al.[35] used surface force measurements in combination with advancing contact angle studies to investigate the PNIPAM chain collapse as a function of molecular weight and grafting densities, the range of which is comparable to our samples. The results appear to indicate that the swollen PNIPAM brush adopts a two-layer structure with a compressible *outer* phase and a dense, incompressible *inner* phase. A similar conclusion was drawn by Ma et al.[42] on the basis of an impedance analysis of quartz crystal microbalance data.

Neutron reflectivity measurements enable a quantitative analysis of density distributions throughout polymer films in general. Yim et al.[55] reported neutron reflectivity experiments on PNIPAM brushes at high grafting densities (molecular weight and surface density estimated to be 209000 g/mol and 0.21 nm^{-1}). The authors observe single layer profiles for temperatures below and above the transition. Within a narrow temperature range, a bilayer profile was observed, with a high density layer at the substrate side of the film. As such, their results exhibit good qualitative agreement with our ellipsometry experiments presented here.

The rapid density variation and corresponding thickness change, as shown in Figure 3, is in agreement with the aforementioned contact angle measurements.[35,49] The latter is very sensitive primarily to the outer layer of the grafted polymer films and as such only exhibits a change when the entire film has collapsed (see also Figure 4).

As a comparison, the (optical) densities of the corresponding dry films are depicted in Figure 4 by the solid black line. In all samples with different grafting densities, the refractive index of the dry brush is larger than that of the wet brush, while the thickness of the dry film is in all cases smaller. This is in agreement with the swelling of the film, even in its collapsed state at elevated temperatures, which leads to a diluted layer with a lower overall density. The reason for the fact that below the LCST the PNIPAM chains at the substrate side do not swell as much as the outer parts may be a kinetic effect. Alternatively, one can imagine that the driving force for swelling originating from osmotic pressure decays upon moving toward the higher segment density at the substrate film interface, in combination with entropic loss. Of course, also the polydispersity of polymer chains constituting our brush films may contribute to a discernible gradient in the density profile of the swollen PNIPAM films considered in this work.

Summarizing, the similarity between the results of our detailed ellipsometric measurements on a specific PNIPAM brush system and conclusions based on force−distance curves in AFM experiments, surface plasmon resonance spectroscopy, and neutron reflectivity on very similar PNIPAM brush systems demonstrate (i) the potential of using a relatively simple, accessible technique such as spectroscopic ellipsometry in probing polymer films in a truly *in situ* manner, while (ii) we quantitatively characterize the segment density profiles within "grafted from" PNIPAM brushes with relatively high density.

dx.doi.org/10.1021/jp304364m | *J. Phys. Chem. B* 2012, 116, 9261−9268

CONCLUSIONS

Using *in situ* spectroscopic ellipsometry, we have studied the temperature-induced collapse transition of "grafted from" PNIPAM films with varying grafting densities. The optical properties of the layers in contact with an aqueous solvent were characterized both at temperatures above and below the LCST (approximately 32−33 °C). The optical response could be modeled in a satisfactory way. Due to an interrelation of the thickness and the refractive index, the best qualitative results were obtained for medium and high grafting densities.

At temperatures below the LCST, the grafted PNIPAM molecular films were swollen considerably. As a result, the density of these diluted layers is comparable to that of water, and as such difficult to model. Nevertheless, we were able to adequately fit our results in terms of a two-layer model. At the substrate/film interface, an optically dense film is considered, on top of which we assume a more diluted layer with a gradient density profile. Upon crossing the LCST, the collapse of the film gives rise to a single layer with a larger density, which could be described adequately with a homogeneous refractive index. Surprisingly, the thickness variations for the medium and high density films scale with a fixed factor of 1.7.

On the basis of our results, we have been able to characterize the configurational changes within the layers as a result of varying temperature in the solution. The diluted layer with an exponentially graded density profile already starts to show changes in the temperature range 25−30 °C, with the most pronounced collapse in the range 30−33 °C. In the same temperature range as where the dilute layer vanishes, the dense layer at the substrate side becomes more dense and exhibits a marked increase in thickness. The density profiles of the films as derived from the ellipsometry spectra were compared with and discussed in relation to similar data obtained from neutron reflectivity measurements. Our results obtained on a specific class of immobilized PNIPAM films demonstrate the power of ellipsometry in general to quantitatively investigate responsive polymers in a truly *in situ* manner.

ASSOCIATED CONTENT

Supporting Information

Ellipsometry spectra for HD, MD, and LD samples below and above the LCST. Details on the modeling of the ellipsometry spectra, including the temperature dependence of the fitting parameters used in the model. This material is available free of charge via the Internet at http://pubs.acs.org.

AUTHOR INFORMATION

Corresponding Author

*E-mail: e.s.kooij@utwente.nl (E.S.K.); g.j.vancso@utwente.nl (G.J.V.). Phone: +31534893148 (E.S.K.); +31534892967 (G.J.V.). Fax: +31534891101 (E.S.K.); +31534893823 (G.J.V.).

Notes

The authors declare no competing financial interest.

ACKNOWLEDGMENTS

This work was financially supported by the MESA+ Institute for Nanotechnology of the University of Twente and The Netherlands Organization for Scientific Research (NWO, TOP Grant 700.56.322, Macromolecular Nanotechnology with Stimulus Responsive Polymers).

REFERENCES

(1) Barbey, R.; Lavanant, L.; Paripovic, D.; Schuwer, N.; Sugnaux, C.; Tugulu, S.; Klok, H. A. *Chem. Rev.* **2009**, *109*, 5437−5527.
(2) Mendes, P. M. *Chem. Soc. Rev.* **2008**, *37*, 2512−2529.
(3) Edmondson, S.; Osborne, V. L.; Huck, W. T. S. *Chem. Soc. Rev.* **2004**, *33*, 14−22.
(4) Matyjaszewski, K.; Tsarevsky, N. V. *Nat. Chem.* **2009**, *1*, 276−288.
(5) Minko, S. *Polym. Rev.* **2006**, *46*, 397−420.
(6) Cohen-Stuart, M. A.; Huck, W. T. S.; Genzer, J.; Muller, M.; Ober, C.; Stamm, M.; Sukhorukov, G. B.; Szleifer, I.; Tsukruk, V. V.; Urban, M.; Winnik, F.; Zauscher, S.; Luzinov, I.; Minko, S. *Nat. Mater.* **2010**, *9*, 101−113.
(7) Tsujii, Y.; Ohno, K.; Yamamoto, S.; Goto, A.; Fukuda, T. *Adv. Polym. Sci.* **2006**, *197*, 1−45.
(8) Sui, X. F.; Zapotoczny, S.; Benetti, E. M.; Schön, P.; Vancso, G. J. *J. Mater. Chem.* **2010**, *20*, 4981−4993.
(9) Smidsrod, O.; Guillet, J. E. *Macromolecules* **1969**, *2*, 272−277.
(10) Schild, H. G. *Prog. Polym. Sci.* **1992**, *17*, 163−249.
(11) Sui, X. F.; Zapotoczny, S.; Benetti, E. M.; Memesa, M.; Hempenius, M. A.; Vancso, G. J. *Polym. Chem.* **2011**, *2*, 879−884.
(12) Tanaka, F.; Koga, T.; Kojima, H.; Winnik, F. M. *Macromolecules* **2009**, *42*, 1321−1330.
(13) Tanaka, F.; Koga, T.; Kojima, H.; Xue, N.; Winnik, F. M. *Macromolecules* **2011**, *44*, 2978−2989.
(14) Tanaka, F.; Koga, T.; Winnik, F. M. *Phys. Rev. Lett.* **2008**, *101*, 028302.
(15) Sui, X. F.; Di Luca, A.; Gunnewiek, M. K.; Kooij, E. S.; van Blitterswijk, C. A.; Moroni, L.; Hempenius, M. A.; Vancso, G. J. *Aust. J. Chem.* **2011**, *64*, 1261−1268.
(16) Xu, F. J.; Zhong, S. P.; Yung, L. Y. L.; Kang, E. T.; Neoh, K. G. *Biomacromolecules* **2004**, *5*, 2392−2403.
(17) Mitsuishi, M.; Koishikawa, Y.; Tanaka, H.; Sato, E.; Mikayama, T.; Matsui, J.; Miyashita, T. *Langmuir* **2007**, *23*, 7472−7474.
(18) Alem, H.; Duwez, A. S.; Lussis, P.; Lipnik, P.; Jonas, A. M.; Demoustier-Champagne, S. *J. Membr. Sci.* **2008**, *308*, 75−86.
(19) Loguka, I.; Wang, X.; Bohn, P. W. *Langmuir* **2007**, *23*, 305−311.
(20) Alexander, S. *J. Phys. (Paris)* **1977**, *38*, 983−987.
(21) de Gennes, P. G. *Macromolecules* **1980**, *13*, 1069−1075.
(22) de Gennes, P. G. *Adv. Colloid Interface Sci.* **1987**, *27*, 189−209.
(23) Cosgrove, T.; Heath, T.; van Lent, B.; Leermakers, F.; Scheutjens, J. *Macromolecules* **1987**, *20*, 1692−1696.
(24) Millner, S. T.; Witten, T. A.; Cates, M. E. *Macromolecules* **1988**, *21*, 2610−2619.
(25) Guiselin, O. *Europhys. Lett.* **1992**, *17*, 225−230.
(26) Tagit, O.; Tomczak, N.; Vancso, G. J. *Small* **2008**, *4*, 119−126.
(27) Synytska, A.; Svetushkina, E.; Puretskyi, N.; Stoychev, G.; Berger, S.; Ionov, L.; Bellmann, C.; Eichhorn, K. J.; Stamm, M. *Soft Matter* **2010**, *6*, 5907−5914.
(28) Ishida, N.; Biggs, S. *Macromolecules* **2010**, *43*, 7269−7276.
(29) Benetti, E. M.; Zapotoczny, S.; Vancso, G. J. *Adv. Mater.* **2007**, *19*, 268−271.
(30) Cole, M. A.; Voelcker, N. H.; Thissen, H.; Horn, R. G.; Griesser, H. J. *Soft Matter* **2010**, *6*, 2657−2667.
(31) Cho, E. C.; Kim, Y. D.; Cho, K. *J. Colloid Interface Sci.* **2005**, *286*, 479−486.
(32) Kidoaki, S.; Ohya, S.; Nakayama, Y.; Matsuda, T. *Langmuir* **2001**, *17*, 2402−2407.
(33) Kaholek, M.; Lee, W. K.; Ahn, S. J.; Ma, H. W.; Caster, K. C.; LaMattine, B.; Zauscher, S. *Chem. Mater.* **2004**, *16*, 3688−3696.
(34) Mendez, S.; Andrzejewski, B. P.; Canavan, H. E.; Keller, D. J.; McCoy, J. D.; Lopez, G. P.; Curro, J. G. *Langmuir* **2009**, *25*, 10624−10632.
(35) Plunkett, K. N.; Zhu, X.; Moore, J. S.; Leckband, D. E. *Langmuir* **2006**, *22*, 4259−4266.
(36) Malham, I. B.; Bureau, L. *Langmuir* **2010**, *26*, 4762−4768.
(37) Zhu, X.; Yan, C.; Winnik, F. M.; Leckband, D. *Langmuir* **2007**, *23*, 162−169.

(38) Yim, H.; Kent, M. S.; Mendez, S.; Lopez, G. P.; Satija, S.; Seo, Y. *Macromolecules* **2006**, *39*, 3420−3426.
(39) Wang, W.; Kaune, G.; Perlich, J.; Papadakis, C. M.; Koumba, A. M. B.; Laschewsky, A.; Schlage, K.; Rohlsberger, R.; Roth, S. V.; Cubitt, R.; Muller-Buschbaum, P. *Macromolecules* **2010**, *43*, 2444−2452.
(40) Ishida, N.; Biggs, S. *Langmuir* **2007**, *23*, 11083−11088.
(41) Liu, G. M.; Zhang, G. Z. *J. Phys. Chem. B* **2005**, *109*, 743−747.
(42) Ma, H. W.; Fu, L.; Li, W.; Zhang, Y. Z.; Li, M. W. *Chem. Commun.* **2009**, 3428−3430.
(43) Naini, C. A.; Franzka, S.; Frost, S.; Ulbricht, M.; Hartmann, N. *Angew. Chem., Int. Ed.* **2011**, *50*, 4513−4516.
(44) Bittrich, E.; Burkert, S.; Muller, M.; Eichhorn, K. J.; Stamm, M.; Uhlmann, P. *Langmuir* **2012**, *28*, 3439−3448.
(45) Xue, C. Y.; Yonet-Tanyeri, N.; Brouette, N.; Sferrazza, M.; Braun, P. V.; Leckband, D. E. *Langmuir* **2011**, *27*, 8810−8818.
(46) Patra, L.; Vidyasagar, A.; Toomey, R. *Soft Matter* **2011**, *7*, 6061−6067.
(47) Rahane, S. B.; Floyd, J. A.; Metters, A. T.; Kilbey, S. M. *Adv. Funct. Mater.* **2008**, *18*, 1232−1240.
(48) Schmaljohann, D.; Nitschke, M.; Schulze, R.; Eing, A.; Werner, C.; Eichhorn, K. J. *Langmuir* **2005**, *21*, 2317−2322.
(49) Balamurugan, S.; Mendez, S.; Balamurugan, S. S.; O'Brien, M. J.; Lopez, G. P. *Langmuir* **2003**, *19*, 2545−2549.
(50) Harmon, M. E.; Jakob, T. A. M.; Knoll, W.; Frank, C. W. *Macromolecules* **2002**, *35*, 5999−6004.
(51) Schmaljohann, D.; Beyerlein, D.; Nitschke, M.; Werner, C. *Langmuir* **2004**, *20*, 10107−10114.
(52) Nerapusri, V.; Keddie, J. L.; Vincent, B.; Bushnak, I. A. *Langmuir* **2006**, *22*, 5036−5041.
(53) Cordeiro, A. L.; Zimmermann, R.; Gramm, S.; Nitschke, M.; Janke, A.; Schäfer, N.; Grundke, K.; Werner, C. *Soft Matter* **2009**, *5*, 1367−1377.
(54) Yim, H.; Kent, M. S.; Mendez, S.; Balamurugan, S. S.; Balamurugan, S.; Lopez, G. P.; Satija. *Macromolecules* **2004**, *37*, 1994−1997.
(55) Yim, H.; Kent, M. S.; Satija; Mendez, S.; Balamurugan, S. S.; Balamurugan, S.; Lopez, G. P. *Phys. Rev. E* **2005**, *72*, 051801.
(56) Zhulina, E. B.; Borisov, O. V.; Pryamitsyn, V. A.; Birshtein, T. M. *Macromolecules* **1991**, *24*, 140−149.
(57) Gao, X.; Kucerka, N.; Nieh, M. P.; Katsaras, J.; Zhu, S. P.; Brash, J. L.; Sheardown, H. *Langmuir* **2009**, *25*, 10271−10278.
(58) Edmondson, S.; Nguyen, N. T.; Lewis, A. L.; Armes, S. P. *Langmuir* **2010**, *26*, 7216−7226.
(59) Tu, H.; Heitzman, C. E.; Braun, P. V. *Langmuir* **2004**, *20*, 8313−8320.
(60) Wang, S. Q.; Zhu, Y. X. *Langmuir* **2009**, *25*, 13448−13455.
(61) Ramos, J. J. I.; Moya, S. E. *Macromol. Rapid Commun.* **2011**, *32*, 1972−1978.
(62) Sui, X. F.; Chen, Q.; Hempenius, M. A.; Vancso, G. J. *Small* **2011**, *7*, 1440−1447.
(63) Zdyrko, B.; Iyer, K. S.; Luzinov, I. *Polymer* **2006**, *47*, 272−279.
(64) Azzam, R. M. A.; Bashara, N. M. *Ellipsometry and polarized light*; Elsevier: Amsterdam, The Netherlands, 1977.
(65) Palik, E. D. *Handbook of Optical Constants of Solids II*; Academic Press: Boston, MA, 1991.
(66) Laloyaux, X.; Mathy, B.; Nysten, B.; Jonas, A. M. *Langmuir* **2010**, *26*, 838−847.